AIP Applied Physics Letters

Nanoscale mechanical switching of ferroelectric polarization via flexoelectricity

Yijia Gu, Zijian Hong, Jason Britson, and Long-Qing Chen

Citation: Applied Physics Letters **106**, 022904 (2015); doi: 10.1063/1.4905837
View online: http://dx.doi.org/10.1063/1.4905837
View Table of Contents: http://scitation.aip.org/content/aip/journal/apl/106/2?ver=pdfcov
Published by the AIP Publishing

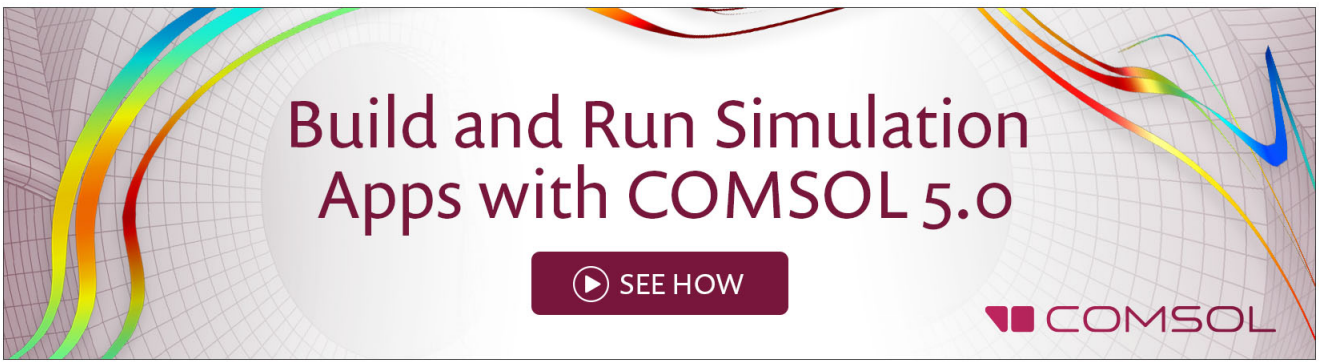

Nanoscale mechanical switching of ferroelectric polarization via flexoelectricity

Yijia Gu, Zijian Hong, Jason Britson, and Long-Qing Chen
Department of Materials Science and Engineering, The Pennsylvania State University, University Park, Pennsylvania 16802, USA

(Received 14 December 2014; accepted 26 December 2014; published online 13 January 2015)

Flexoelectric coefficient is a fourth-rank tensor arising from the coupling between strain gradient and electric polarization and thus exists in all crystals. It is generally ignored for macroscopic crystals due to its small magnitude. However, at the nanoscale, flexoelectric contributions may become significant and can potentially be utilized for device applications. Using the phase-field method, we study the mechanical switching of electric polarization in ferroelectric thin films by a strain gradient created via an atomic force microscope tip. Our simulation results show good agreement with existing experimental observations. We examine the competition between the piezoelectric and flexoelectric effects and provide an understanding of the role of flexoelectricity in the polarization switching. Also, by changing the pressure and film thickness, we reveal that the flexoelectric field at the film bottom can be used as a criterion to determine whether domain switching may happen under a mechanical force. © *2015 AIP Publishing LLC*. [http://dx.doi.org/10.1063/1.4905837]

The emergence of nanotechnology has revolutionarily changed the discipline of material science and engineering. It either utilizes the quantum effect or takes advantage of the great surface-to-volume ratio to tune the properties of materials at the nanoscale. The quantum effect enables the material characteristic size-dependent phenomenon including quantum confinement, tunneling, quantum transport, etc. The surface-to-volume ratio, which is inversely proportional to the length scale, is the key for highly efficient catalysis and ultrastrong alloys with high ductility.[1] The gradient effect, which is also inversely proportional to the length scale, may become significant at nanometer scale and thus dramatically change material properties and performance. However, it has not drawn much attention in contrast to the other two aspects of nanomaterials.

Flexoelectricity, as one of such effects depending on the gradient, measures the coupling between the gradient of mechanical strain and the electric polarization. Therefore, together with the well-known piezoelectricity, the dependence of induced electric polarization on mechanical deformation can be phenomenologically written as

$$P_i = e_{ijk}\varepsilon_{jk} + \mu_{ijkl}\frac{\partial \varepsilon_{kl}}{\partial x_j}, \tag{1}$$

where ε_{ij} is the strain component, e_{ijk} is the third-rank piezoelectric tensor, and μ_{ijkl} is the fourth-rank flexoelectric (polarization) tensor. The first term on the right-hand side of Eq. (1) describes the piezoelectric effect, i.e., the linear response of polarization to a homogeneous applied strain. The second term is the flexoelectric contribution to polarization from an inhomogeneous strain, i.e., strain gradient. While piezoelectricity only exists in crystals without inversion symmetry, flexoelectricity exists in all crystals.

The piezoelectricity is a very well studied effect, and it has already been utilized in many device applications including actuators, sensors, and microelectromechanical systems (MEMSs).[2,3] In contrast, the flexoelectricity is much less understood. As a matter of fact, it is usually neglected in macroscale systems since the magnitude of flexoelectric coefficient μ_{ijkl} is typically on the order of nC/m.[4] However, at the nanoscale, the strain gradient can approach $\sim 10^6$–$10^7\,\mathrm{m}^{-1}$, and as a result the flexoelectric effect becomes significant or even dominant over the piezoelectric effect.

There are ample evidences demonstrating the existence of flexoelectric effect. For example, the domain walls, across which the strain varies over a nanometer thickness, are natural candidates for significant flexoelectricity effects. It was recently shown theoretically that both twin walls and antiphase boundaries in the incipient ferroelectric $SrTiO_3$ (STO) have non-zero polarization due to the flexoelectric effect.[5,6] The long-believed Ising-like 180° domain walls in tetragonal ferroelectrics were of mixed Néel and Bloch character due to flexoelectricity.[7–9]

The flexoelectric effect can also be utilized to switch ferroelectric domains through a mechanical force rather than an electric field. Recently, Lu *et al*. demonstrated the strain gradient generated by an atomic force microscopy (AFM) tip can mechanically switch the polarization within a nanoscale volume of a ferroelectric film.[10] However, there are fundamental questions with regard to this experimental demonstration. For example, since the stress induced by AFM is huge, the piezoelectric effect is not negligible. An interesting question arises as to what are the relative contributions from piezoelectricity and flexoelectricity in the switching process. If the switching is dominated by flexoelectric effect, what is the critical limit for the thickness of the film and the magnitude of load? In this paper, we use the phase-field method to investigate and understand the mechanical writing process.

We first extended the phase-field model of ferroelectric domains[11,12] to include the flexoelectric contributions. The free energy density of a ferroelectric crystal is given by[13]

$$F = \alpha_{ij}P_iP_j + \alpha_{ijkl}P_iP_jP_kP_l + \alpha_{ijklmn}P_iP_jP_kP_lP_mP_n + \alpha_{ijklmnor}P_iP_jP_kP_lP_mP_nP_oP_r + \frac{1}{2}g_{ijkl}\frac{\partial P_i}{\partial x_j}\frac{\partial P_k}{\partial x_l} + \frac{1}{2}c_{ijkl}\varepsilon_{ij}\varepsilon_{kl} - q_{ijkl}\varepsilon_{ij}P_kP_l + \frac{f_{ijkl}}{2}\left(\frac{\partial P_k}{\partial x_l}\varepsilon_{ij} - \frac{\partial \varepsilon_{ij}}{\partial x_l}P_k\right) - P_i\left(E_i + \frac{E_i^d}{2}\right), \quad (2)$$

where x_i is the ith component of the Cartesian coordinate system, P_i is the polarization component, ε_{ij} is the stress component, E_i is the applied electric field, E_i^d is the depolarization field, α's are the dielectric stiffness tensor (only α_{ij} is assumed to be temperature dependent), g_{ijkl} is the gradient energy coefficient, c_{ijkl} is the elastic stiffness tensor, q_{ijkl} is the electrostrictive tensor, and f_{ijkl} is the flexoelectric (polarization) tensor.[14] By minimizing the total free energy Eq. (2) with respect to polarization, we get

$$P_j = \frac{1}{2\alpha_{ij} - q_{ijkl}\varepsilon_{kl}}\left(f_{ijkl}\frac{\partial \varepsilon_{kl}}{\partial x_j} + E_i + E_i^d\right) = \varepsilon_0\chi_{ij}\left(E_i^f + E_i + E_i^d\right), \quad (3)$$

where ε_0 is the permittivity of vacuum, χ_{ij} is the dielectric constant, and $E_i^f = f_{ijkl}(\partial\varepsilon_{kl}/\partial x_j)$ is the flexoelectric field.[14] (Higher order terms of P polynomials are ignored for simplicity.) Thus, the flexoelectric effect can be regarded as an analogue to the electric field, which can modify the free energy profile asymmetrically in contrast to homogeneous stress.[10] Its magnitude and direction are dependent on the flexoelectric tensor and the strain gradient component.

The temporal evolution of the three-dimensional polarization field (P_i, $i = 1$, 2, and 3) is described by time-dependent Ginzburg-Landau (TDGL) equation

$$\frac{\partial P_i(\mathbf{r},t)}{\partial t} = -L\frac{\delta F}{\delta P_i(\mathbf{r},t)} \quad (i = 1,2,3), \quad (4)$$

where L is a kinetic coefficient related to the domain wall mobility and $\mathbf{r}$ is the position. The stress distribution under the AFM tip is approximated by a spherical indenter, i.e.,

$$\sigma_{33} = -\frac{3p}{2\pi a^2}\sqrt{1 - \frac{r^2}{a^2}}, \quad (5)$$

where r is the distance from the tip-surface junction, p is the load, and a is the radius of contact area (as shown in Fig. 1(a)). The latter is proportional related to $p^{1/3}$.[15]

In order to compare with the previous experimental results,[10] compressively strained ultrathin $BaTiO_3$ (BTO) thin films are studied. The simulation setups are chosen to be similar to the experimental conditions.[10] The BTO film thickness was assumed to be 5 nm (12 unit cells). The STO substrate was assumed to exert a biaxial 2.5% compressive strain on BTO layer. The coefficients of BTO for Eq. (2) are from Refs. 16, 17 to 18. The flexoelectric coefficients are scaled with a factor of 0.6, considering the dielectric constant difference between $Ba_{0.5}Sr_{0.5}TiO_3$ and BTO.[18] Under this condition, the equilibrium structure of the BTO film (with no load) is tetragonal with a uniaxial spontaneous polarization of 0.34 C/m^2. The radius of the contact area can be estimated from the observed domain width to be about 10 nm with a 1000 nN load.[10]

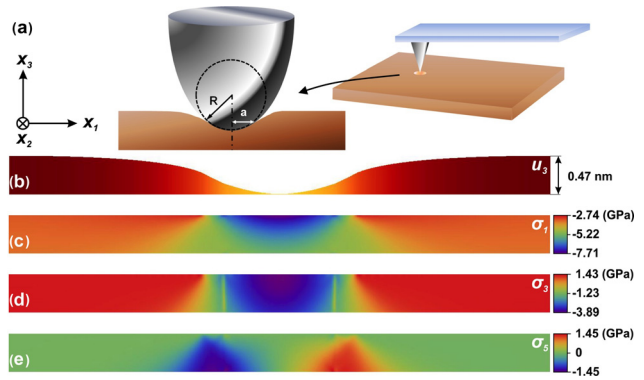

FIG. 1. Mechanical writing on thin film via AFM tip (spherical indenter). (a) The schematic setup of the system. R is the radius of the AFM tip sphere (dashed circle). a is the radius of the contact area. (b) Surface displacement of the cross-section. (c)–(e) Distribution of stress components σ_1, σ_3, and σ_5.

TDGL Eq. (4) were solved using the semi-implicit Fourier spectral method[12] on a $1024\Delta x \times 1\Delta x \times 512\Delta x$ mesh with periodic boundary conditions along the $x_1$and x_2 axes, where $\Delta x = 69.06$ pm is the simulation grid spacing. To solve Eqs. (2) and (4) accurately, a finite difference method was used to calculate the out-of-plane derivatives of the polarization and strain in Eq. (2) and the results used to correct the spectral method in an approach broadly similar to that proposed by Wangüemert-Pérez *et al.*[19] This approach greatly reduces the large oscillations in the derivative functions near the thin film boundaries associated with the Gibbs phenomenon that arise due to the discontinuous changes in these functions at the film edges. The thicknesses of the ferroelectric thin film and STO substrate were taken to be $72\Delta x$ and $284\Delta x$, respectively. For the electrostatic energy calculations, we used background dielectric constants of 45.[20] To simulate the thin film with mechanical load, mixed boundary conditions were used, in which the displacement at the bottom of the substrate was assumed to be zero and the top surface of the film was assumed to be traction free in the absence of the indenter. Under the AFM indenter, the σ_{33} stress was assumed to be non-zero. Boundary conditions in the out-of-plane direction were applied using a superposition solution method.[21]

The simulation started from small random noises with $P_3 > 0$. Without load, the equilibrium structure was a single c domain with out-of-plane polarization component $P_3 = 0.34$ C/m^2, which is identical to the previous thermodynamic calculation. Then with an AFM load of 1000 nN, the system with the same initial condition was relaxed to equilibrium. The calculated surface displacement and stress distribution are shown in Figures 1(b)–1(e). The radius of the contact area is 10 nm and the maximum displacement of the top surface is around 0.47 nm. As shown in Figures 1(c)–1(e), huge compressive stresses (both in-plane and out-of-plane) are induced by the AFM. Within the contact region, the stress variations under AFM tip are over several GPa, which is well above the coercive stresses. In addition, the flexoelectric field induced by the AFM tip reaches as

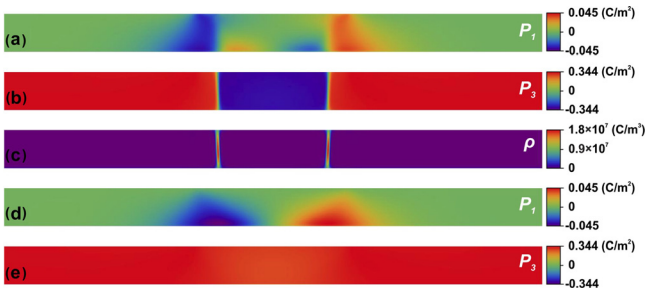

FIG. 2. The polarization distribution under mechanical load 1000 nN. (a) and (b) The polarization component P_1 and P_3 with flexoelectric effect, (c) the bound change induced by the wedged domain walls, (d) and (e) the polarization component P_1 and P_3 without flexoelectric effect.

high as 10^7 V/m, which is well above the coercive field of BTO ($\sim 10^6$ V/m) as well.

Because the coercive fields and stresses from the Landau-Ginzburg-Devonshire theory are typically much larger than the experimental measurements (for example, the coercive field is usually more than ten times larger than the experimental observed values partially due to the existence of defects), the real switching barrier should be much lower than the calculated values from the phase-field simulation. Therefore, the simulation starts from noises with positive out-of-plane polarization component P_3 to reduce the switching barrier; the final relaxed states thus represent the switched equilibrium domain structures. It should be noted that the calculated flexoelectric field is based on constant flexoelectric coupling coefficients, i.e., the stress-induced variation of dielectric permittivity is not considered here.

The calculated polarization distribution is shown in Figure 2. It is found that the volume under AFM tip has been switched with the out-of-plane polarization component pointing down. There exists in-plane polarization components as well, induced by the deformation. The magnitudes for the in-plane components are, however, an order of magnitude smaller than the out-of-plane component. That is, because the substrate constraint is so large that the formation of in-plane domains is inhabited. An interesting phenomenon is the appearance of wedged domain walls. As shown in Figures 2(a) and 2(b), the domain walls are not parallel to x_3, there must be bound charge near the domain walls (Figure 2(c)). The calculated bound charge density reaches as high as 10^7 C/m^3. The induced bound charge may interact with the carriers and modify their mobility and thus the local electric conductivity. This might be one of the reasons that the resistivity change of direct electric switching of polarization is smaller than that from mechanical switching via flexoelectricity.[22]

One advantage of the phase-field method is the fact that one can easily separate the contributions of different driving forces to polarization switching and understand their relative roles in the switching mechanism. By setting the flexoelectric coefficients to zero, we turned off the flexoelectric effect. Thus, the polarization change is entirely due to the piezoelectric effect. The polarization distribution with only including piezoelectric contributions is shown in Figures 2(d) and 2(e). As compared to Figures 2(a) and 2(b), the distribution of polarization components is quite different. The major difference is no switched *c* domain. The out-of-plane polarization component P_3 under tip is compressed but not switched. This can be explained by how these two types of deformation-polarization coupling modify the free energy profile. As illustrated in Figure 3(a), the flexoelectric effect is similar to that by an electric field which changes the free energy profile asymmetrically. If the flexoelectric field is large enough to overcome the energy barrier, the polarization flips. In contrast, the piezoelectric effect modifies the free energy symmetrically (Figure 3(b)). The equilibrium polarization may be extended or compressed but not 180° switched. Thus, we conclude that *the polarization flipping by mechanical deformation is due to the flexoelectric effect*. The piezoelectric effect is comparably weak but should not be neglected. By comparing Figures 2(b) and 2(e), the in-plane components show some similarities. They have similar magnitude and both exhibit the highest value at the film-substrate interface.

The film thickness and load are two other factors that may affect the flexoelectric effect. Apparently, a small load cannot provide sufficiently high flexoelectric fields to switch the ferroelectric domains. On the other hand, thick films cannot exhibit strong flexoelectric effects as well, even though the strain gradient just under the AFM tip may still be very large. To study the dependence of domain switching on film thickness, we performed a series of phase-field simulations by varying both film thickness and the applied load. The simulation results are plotted in Figure 4(a). The switched domain width remains almost constant and suddenly drops when the film reaches the critical thickness for each fixed load. Figures 4(b)–4(e) show the polarization, stress

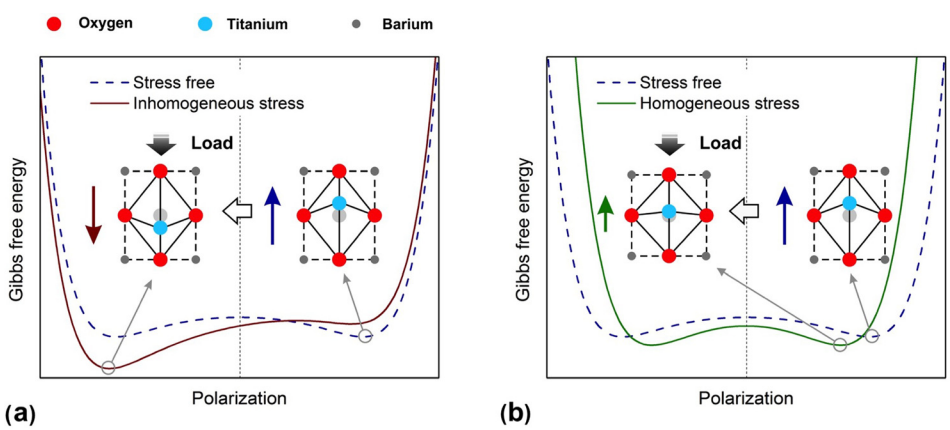

FIG. 3. The energy profile change as the effect of different polarization and deformation coupling: (a) flexoelectricity and (b) piezoelectricity. The solid arrows indicate the polarization magnitude and direction.

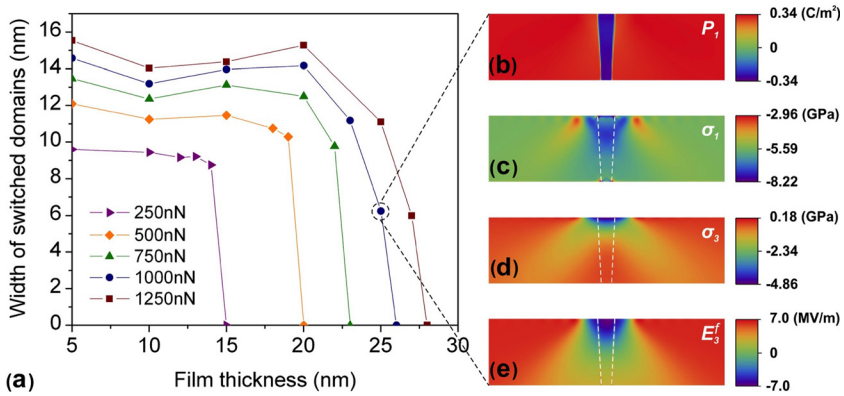

FIG. 4. The thickness dependence of mechanical switching via flexoelectric effect. (a) Switched domain width on the top surface of the film as a function of film thickness and applied load. The profiles of out-of-plane polarization component P_3 (b), stress components σ_1 (c) and σ_3 (d), and out-of-plane flexoelectric field (e) at 1000 nN of a film of 25 nm thick. The white dashed lines indicate the switched domain.

components, and the flexoelectric field distribution of a film with 25 nm thick under a 1000 nN load. The switched domain is about 6 nm wide, which is well within the contact area of 10 nm width. As shown in Figure 4(e), the flexoelectric effect far from the tip-surface junction becomes too weak to switch the local polarization. Only near the center, the flexoelectric field is strong enough to switch the polarization. When the film is too thick to produce a strong flexoelectric field to switch the polarization in the region at the bottom of the film, the domain switching cannot happen at all since the huge electrostatic energy penalty inhibits the formation of partial domains. In other words, the flexoelectric effect induced switching must penetrate the whole film thickness. Therefore, in order to have flexoelectric-effect-induced domain switching, the critical film needs to be so thin that the flexoelectric field at the film-substrate interface is still larger than the coercive field. This can well explain why the flexoelectric effect induced switching is not observed in thick films or bulk materials.

It should be pointed out that there are still no reliable values for the flexoelectric coefficients for BTO. For example, the flexoelectric coefficients of BTO obtained from experimental measurements[23] and theoretical calculations[18,24] are several orders of magnitude different. The experimentally measured flexoelectric coefficients may be affected by different boundary conditions,[25] surface piezoelectricity, and surface flexoelectricity.[24] Therefore, in this work, we adopt the values from first-principles calculations.[18]

In addition to the uncertainty in the flexoelectric coefficients, the shape of the AFM tip is another factor that may affect our simulation results. In the following, we also simulated a flat punch-like AFM tip to compare with spherical indenter geometry. To be specific, we calculated the three-dimensional flexoelectric field distribution from two quite

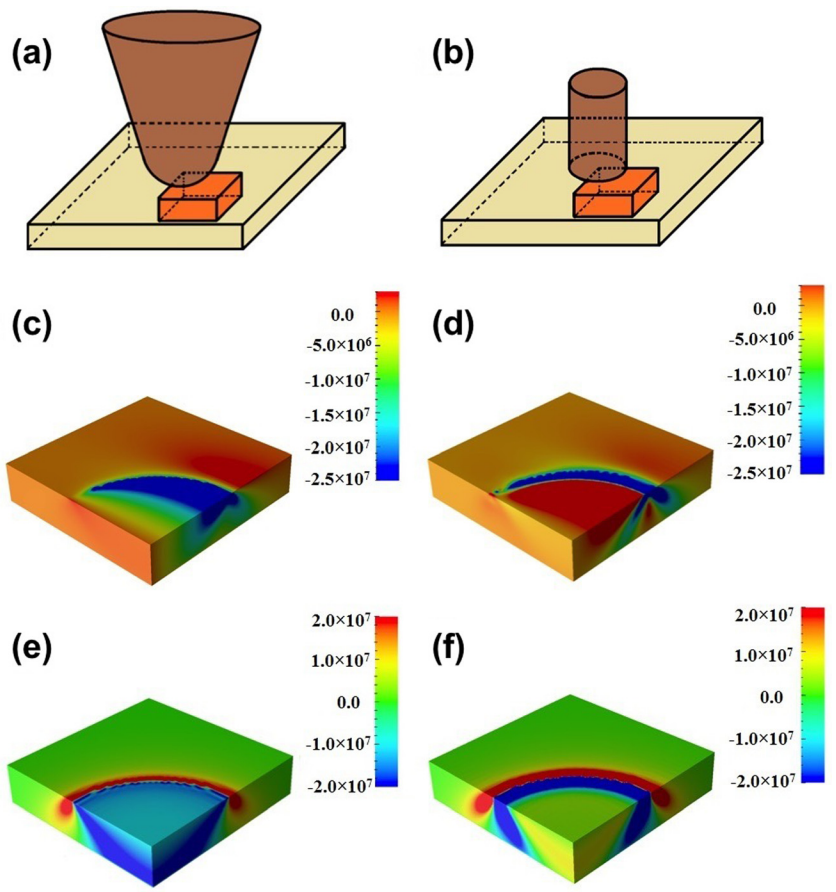

FIG. 5. The flexoelectric field distributions for different AFM tip geometries (unit: V/m): spherical indenter (a) schematic, (c) in-plane flexoelectric field E_1^f, (e) out-of-plane flexoelectric field E_3^f; cylindrical flat punch (b) schematic (d) in-plane flexoelectric field E_1^f, (f) out-of-plane flexoelectric field E_3^f.

different tip geometries. For the flat punch-like tip geometry, a 12th-order polynomial is used to represent a nearly flat bottom. The displacement on the top surface induced by the additional stress is written as[26]

$$\delta(r) = \frac{br^{12}}{12}, \; r \le a, \tag{6}$$

where b is a fitting constant. We adopted a mesh size of $200 \times 200 \times 30$, simulating a real size of $80\,\text{nm} \times 80\,\text{nm} \times 12\,\text{nm}$, in which the film thickness and the substrate thickness were all set as 4.8 nm. For the two tips, loads were chosen to be 1000 nN in each case. Figure 5 shows the quarter plot of the flexoelectric field distributions from the calculation zoomed near the tip center with a size of $20\,\text{nm} \times 20\,\text{nm} \times 4.5\,\text{nm}$. Both tip geometries show similar strong flexoelectric fields in both x_1 and x_3 directions, which are well above the coercive fields of BTO thin film. The fields change dramatically at the contact edges due to the sharp variation of the stresses. Both tip geometries show that the out-of-plan flexoelectric field E_3^f at the bottom are still large enough to overcome the switching barrier. Therefore, we conclude that the AFM tip geometry is not important comparing to film thickness and the stress in the mechanical switching process.

In this letter, we present a phase-field model of ferroelectric domains with flexoelectric contribution. We reproduced the mechanical switching process under an AFM approximated as a spherical tip indenter. The flexoelectric effect is shown to be strongly localized. The flexoelectric field reaches as high as $\sim 10^7$ V/m beneath the AFM tip and decays quickly away from the tip. This type of mechanical switching is only possible in nanoscale films with the upper bound for the film thickness on the order of a few nanometers. The mechanical switching via flexoelectric effect is more similar to electric field induced switching rather than the conventional mechanical switching via piezoelectricity. The switched ferroelectric domains are thermodynamically stable even after unloading. Hence, this switching process has potential applications in high-density data storage via mechanical means, which can avoid leakage or dielectric breakdown as in direct electric switching.

The authors would like to thank Dr. Susan Trolier-McKinstry for her insightful suggestions and acknowledge Dr. Haidong Lu for reading the manuscript. This work was supported by the NSF through Grant Nos. DMR-1210588, DMR-1234096, and DMR 1410714 (Gu and Hong) and US Department of Energy, Office of Basic Energy Sciences, Division of Materials Sciences and Engineering under Award No. DE-FG02-07ER46417 (Britson). The computer simulations were carried out on the LION and cyberstar clusters at the Pennsylvania State University, in part supported by instrumentation (cyberstar Linux cluster) funded by the NSF through Grant No. OCI-0821527.

[1]Y. Wang, M. Chen, F. Zhou, and E. Ma, Nature **419**, 912–915 (2002).
[2]T. M. Shaw, S. Trolier-McKinstry, and P. C. McIntyre, Annu. Rev. Mater. Sci. **30**, 263–298 (2000).
[3]S. Trolier-McKinstry and P. J. Muralt, Electroceramics **12**, 7–17 (2004).
[4]S. M. Kogan, Sov. Phys.-Solid State **5**, 2069–2070 (1964).
[5]A. N. Morozovska, E. A. Eliseev, S. V. Kalinin, L.-Q. Chen, and V. Gopalan, Appl. Phys. Lett. **100**, 142902 (2012).
[6]A. N. Morozovska, E. A. Eliseev, M. D. Glinchuk, L.-Q. Chen, and V. Gopalan, Phys. Rev. B **85**, 094107 (2012).
[7]Y. Gu, M. Li, A. N. Morozovska, Y. Wang, E. A. Eliseev, V. Gopalan, and L.-Q. Chen, Phys. Rev. B **89**, 174111 (2014).
[8]P. V. Yudin, A. K. Tagantsev, E. A. Eliseev, A. N. Morozovska, and N. Setter, Phys. Rev. B **86**, 134102 (2012).
[9]M. Li, Y. Gu, Y. Wang, L.-Q. Chen, and W. Duan, Phys. Rev. B **90**, 054106 (2014).
[10]H. Lu, J. Alcala, C. B. Eom, G. Catalan, and A. Gruverman, Science **336**, 59–61 (2012).
[11]L.-Q. Chen, Annu. Rev. Mater. Res. **32**, 113–140 (2002).
[12]L.-Q. Chen and J. Shen, Comput. Phys. Commun. **108**, 147–158 (1998).
[13]E. A. Eliseev, A. N. Morozovska, M. D. Glinchuk, and R. Blinc, Phys. Rev. B **79**, 165433 (2009).
[14]W. Ma, Phys. Status Solidi B **245**, 761–768 (2008).
[15]A. C. Fischer-Cripps, *Introduction to Contact Mechanics*, Mechanical Engineering Series, 2nd ed. (Springer, New York, 2007).
[16]J. J. Wang, P. P. Wu, X. Q. Ma, and L. Q. Chen, J. Appl. Phys. **108**, 114105 (2010).
[17]J. Hlinka and P. Márton, Phys. Rev. B **74**, 104104 (2006).
[18]I. Ponomareva, A. K. Tagantsev, and L. Bellaiche, Phys. Rev. B **85**, 104101 (2012).
[19]J. G. Wangüemert-Pérez, R. Godoy-Rubio, A. Ortega-Moñux, and I. Molina-Fernández, J. Opt. Soc. Am. A **24**, 3772–3780 (2007).
[20]G. Rupprecht and R. O. Bell, Phys. Rev. **135**, 748–752 (1964).
[21]Y. Li, S. Hu, Z. Liu, and L.-Q. Chen, Acta Mater. **50**, 395–411 (2002).
[22]H. Lu, D. J. Kim, S. Ryu, C. B. Eom, E. Y. Tsymbal, A. Gruverman, and C. W. Bark, Nano Lett. **12**, 6289–6292 (2012).
[23]W. Ma and L. E. Cross, Appl. Phys. Lett. **88**, 232902 (2006).
[24]R. Maranganti and P. Sharma, Phys. Rev. B **80**, 054109 (2009).
[25]J. Hong and D. Vanderbilt, Phys. Rev. B **88**, 174107 (2013).
[26]V. M. Aleksandrov and D. A. Pozharskii, *Three-Dimensional Contact Problems* (Kluwer Academic Publishers, 2001), p. 420.